Energy tuning of the Electronic Spin Coherent evolution in Methylammonium lead iodide perovskites

Guadalupe Garcia-Arellano[1], Gaëlle Trippé-Allard[2], Laurent Legrand[1], Thierry Barisien[1], Damien Garrot[3], Emmanuelle Deleporte[2], Frédérick Bernardot[1], Christophe Testelin[1] and Maria Chamarro[1]

[1]Sorbonne Université, CNRS, Institut des NanoSciences de Paris, 4 place Jussieu, F-75005 Paris, France

[2]Université Paris-Saclay, ENS Paris-Saclay, Centrale Supélec, CNRS, LuMIn, F-91190 Gif-sur-Yvette, France

[3] Université Paris-Saclay, UVSQ, CNRS, GEMaC, F-78000 Versailles, France..

Supplementary information

1. Temperature dependence of the optical absorption of a $CH_3NH_3PbI_3$ polycrystalline film

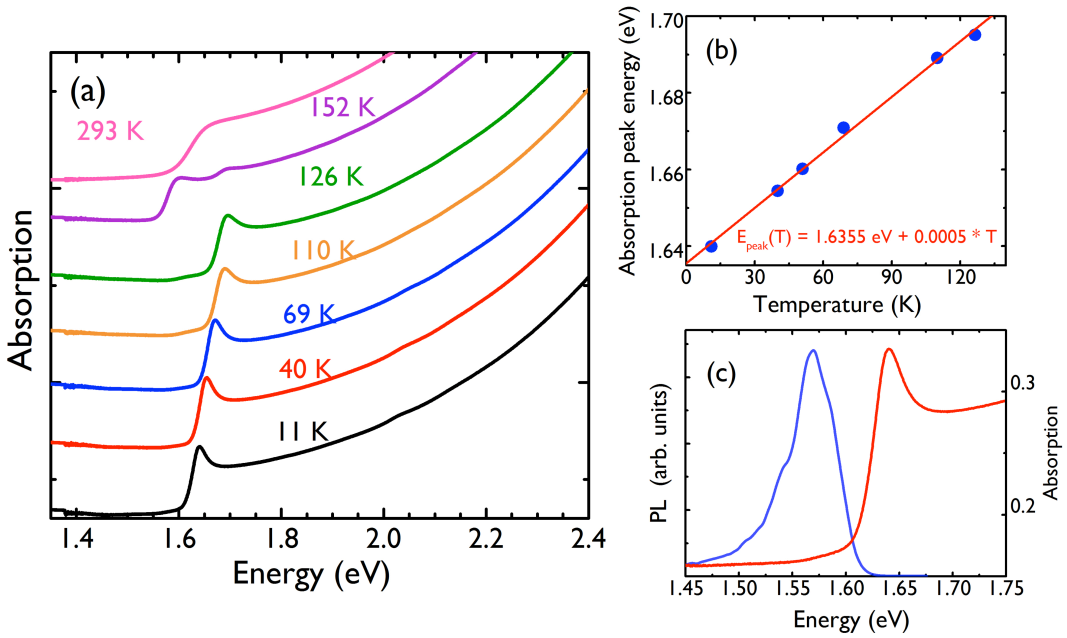

Fig. S1: (a) Absorption spectra at different temperatures in the range 11 - 293 K of a $CH_3NH_3PbI_3$ polycrystalline film. The curves have been shifted for clarity (b) Absorption peak energy as a function of the temperature (blue points) and linear fit (solid red line) of the data. (c) Micro-photoluminescence spectrum performed on MAPI sample at 7 K (blue line), exciting at an energy of 3.1 eV (400nm), and absorption spectrum at 11 K (red line).

2. Fast Fourier transform (FFT) of the PFR signal as a function of the magnetic field, at two different energies.

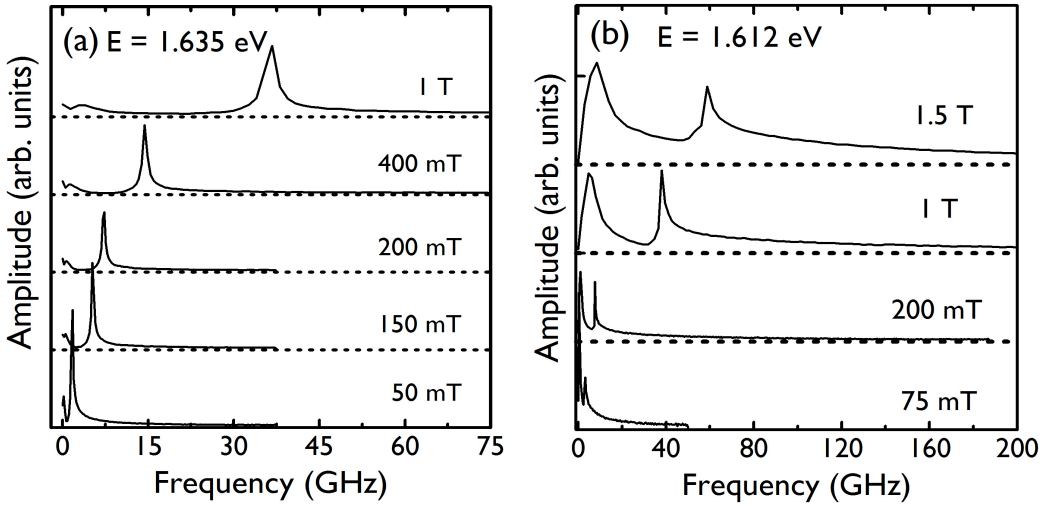

Fig. S2 Fast Fourier transform (FFT) of the PFR signals at different values of the magnetic field, obtained at (a) 1.635 eV and (b) 1.612 eV. The corresponding PFR signals are shown in the main text. The curves have been shifted for clarity; the dotted horizontal lines are based lines.

3. Theoretical support: Exciton fine structure.

At the band gap edge, the wave functions of the conduction states can be written [1]:

$|C_1\rangle = i[-\alpha X_c \downarrow\ -i\beta Y_c \downarrow + \gamma\, Z_c \uparrow]$

$|C_2\rangle = i[\alpha X_c \uparrow\ -i\beta Y_c \uparrow + \gamma\, Z_c \downarrow]$

with $\alpha^2 + \beta^2 + \gamma^2 = 1$. The real constants (α, β, γ) and θ are given in Ref.[2]. In the cubic phase, $\alpha = \beta = -\gamma = \frac{1}{\sqrt{3}}$ and the states $|C_{1(2)}\rangle$ are associate to states with a total kinetic momentum $j_e = \frac{1}{2}: \left|j_e = \frac{1}{2};\ j_z^e = \pm\frac{1}{2}\right\rangle$. In a tetragonal phase, $\alpha = \beta = \frac{cos\theta}{\sqrt{2}}$ and $\gamma = -sin\theta$.

The hole states, present in the valence band, are defined as:

$$|W_1\rangle = S_V \uparrow \qquad \text{and} \qquad |W_2\rangle = S_V \downarrow$$

Four excitonic states can then be formed by electron-hole pairs $|C_i, W_j\rangle$ $(i, j = 1,2)$.

One can define one dark exciton $|O_D\rangle$ and three bright excitons $(|O_B\rangle, |\pm 1\rangle)$:

$$|O_D\rangle = \frac{1}{\sqrt{2}}[|C_1, W_2\rangle - |C_2, W_1\rangle], \quad |O_B\rangle = \frac{1}{\sqrt{2}}[|C_1, W_2\rangle + |C_2, W_1\rangle],$$

$$|+1\rangle = |C_1, W_1\rangle \text{ and } |-1\rangle = |C_2, W_2\rangle.$$

It is also convenient to defined the linearly polarized exciton states:

$$|X\rangle = \frac{|+1\rangle + |-1\rangle}{\sqrt{2}} \quad , \quad |Y\rangle = \frac{|+1\rangle - |-1\rangle}{\sqrt{2}} \quad \text{and} \quad |Z\rangle = |O_B\rangle$$

The electron-hole exchange interaction includes two contributions, the short-range (SR) and the long-range (LR) interaction. The SR (or analytical) contribution can be written as a contact interaction with the electron and hole spin Pauli operators:

$$H_{SR} = \frac{1}{2} C (1 - \sigma_e . \sigma_h)\, \delta(r_e - r_h)$$

The LR (or non-analytical) interaction has been described in Ref. [3]. Both interactions can be derived in the basis formed by the eigenstates $\{|O_D\rangle, |X\rangle, |Y\rangle, |Z\rangle\}$, with respective eigenenergies, in a bulk materials :

$E_0 = 0$

$E_X = (3\Delta_{SR} + 2\Lambda E_{P_{S,\rho}})\beta^2$

$E_Y = (3\Delta_{SR} + 2\Lambda E_{P_{S,\rho}})\alpha^2$

$E_Z = (3\Delta_{SR} + 2\Lambda E_{P_{S,z}})\gamma^2$

with $\Lambda = \frac{1}{3E_g^2}\frac{\hbar^2}{2m_0}\frac{e^2}{\varepsilon_0\varepsilon_X}\frac{1}{\pi a_X^3}$. E_g is the band gap energy, a_X the bulk Bohr radius, m_0 the free electron mass, ε_0 the electric permittivity of vacuum, ε_X the material dielectric constant at the exciton energy and *e* the electron charge, $\Delta_{SR} = \frac{2C}{3\pi a_X^3}$ with *C* estimated in Ref. [3] (*C* = 107.6 meV nm^3)

In the orthorhombic phase, the excitonic degeneracy is totally lifted and the fine structure splitting (FSS) can be defined by the splittings $\delta_{BD} = E_Y - E_0$, $\Delta E_1 = E_X - E_Y$ and $\Delta E_2 = E_Z - E_Y$ (see Fig. S3-I, D_{2h} symmetry). In the cubic phase, the 3 bright states are degenerate, while in tetragonal phase, the bright states degeneracy is partially lifted (see in Fig. S3-I, the O_h and D_{4h} symmetries).

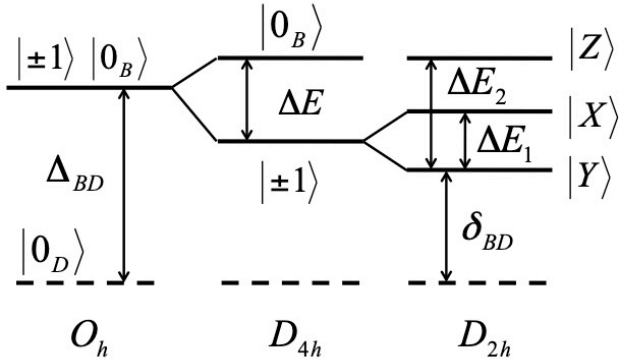

Fig.S3-I Energy labelling of the fine structure exciton states with cubic, tetragonal and orthorhombic symmetry.

For a transverse magnetic field B along the Ox axis, the Zeeman Hamiltonian can be written as:

$$H_Z = \frac{1}{2}\mu_B[g_e\sigma_x^e + g_h\sigma_x^h]B$$

with $\sigma_x^{e/h}$ Pauli operators defined respectively in the basis $\{|C_i\rangle\}$ and $\{|W_j\rangle\}$

In the basis $\{O_D\rangle, |X\rangle, |Y\rangle, |Z\rangle\}$, the Hamiltonian $H = H_{exch} + H_Z$ can be separate in two subspaces :

$\{|O_D\rangle, |Y\rangle\}$ with H defined by the matrix H_1 : $\begin{pmatrix} E_0 & \frac{1}{2}\mu_B(g_h - g_e)B \\ \frac{1}{2}\mu_B(g_h - g_e)B & E_Y \end{pmatrix}$

$\{|Z\rangle, |X\rangle\}$ with H defined by the matrix H_2 : $\begin{pmatrix} E_Z & \frac{1}{2}\mu_B(g_h + g_e)B \\ \frac{1}{2}\mu_B(g_h + g_e)B & E_X \end{pmatrix}$

The eigenenergies and eigenstates of H_1 are then:

$$E_1^{\pm} = \frac{E_0 + E_Y}{2} \pm \frac{1}{2}\sqrt{(E_0 - E_Y)^2 + [\mu_B(g_h - g_e)B]^2}$$

$$\psi_1^+ = cos\varphi|O_D\rangle + sin\varphi|Y\rangle$$

$$\psi_1^- = -sin\varphi|O_D\rangle + cos\varphi|Y\rangle$$

The eigenenergies and eigenstates of H_2 are:

$$E_2^{\pm} = \frac{E_Z + E_X}{2} \pm \frac{1}{2}\sqrt{(E_Z - E_X)^2 + [\mu_B(g_h + g_e)B]^2}$$

$$\psi_2^+ = cos\phi|Z\rangle + sin\phi|X\rangle$$

$$\psi_2^- = -sin\phi|Z\rangle + cos\phi|X\rangle$$

Under a σ^+ circularly polarized excitation, an exciton $|+1\rangle = \frac{|X\rangle + |Y\rangle}{\sqrt{2}}$ is created and is a coherent superposition of the eigenstates of the system. At t = 0, the exciton is in the state:

$$\psi(0) = \frac{1}{\sqrt{2}}\{sin\phi\ \psi_2^+ + cos\phi\psi_2^- + sin\varphi\ \psi_1^+ + cos\varphi\ \psi_1^-\}$$

Knowing the eigenenergies, it is possible to estimate the time evolution of the exciton state $\psi(t)$ and to deduce the z-component of the spin measured in the PFR technique:

$$S_z \propto \frac{1}{2}[|\langle +1|\psi(t)\rangle|^2 - |\langle -1|\psi(t)\rangle|^2]$$

which can be rewritten as:

$$S_z \propto \frac{1}{2}\ [c_1 cos\omega_1 t + c_2 cos\omega_2 t + c_3 cos\omega_3 t + c_4 cos\omega_4 t]$$

with $c_1 = cos^2\varphi cos^2\phi$, $c_2 = cos^2\varphi sin^2\phi$, $c_3 = sin^2\varphi cos^2\phi$, $c_4 = sin^2\varphi sin^2\phi$

and : $h\nu_1 = |E_2^- - E_1^-|$, $h\nu_2 = |E_2^+ - E_1^-|$, $h\nu_3 = |E_2^- - E_1^+|$, $h\nu_4 = |E_2^+ - E_1^+|$

In absence of electron-hole exchange, $h\nu_1 = h\nu_4 = |g_h|\mu_B B$ and $h\nu_2 = h\nu_3 = |g_e|\mu_B B$. Two oscillations are present in the signal and both frequencies are linear in B, $h\nu_{2,3}$ and $h\nu_{1,4}$ being related to the electron and hole Landé factor, respectively. A similar behavior can also

be obtained if the exchange energy is small as compared to the Zeeman splitting, as assumed by Ref.[4] , with $\delta_{BD} = 5\ \mu eV$ and $\Delta E = -1\ \mu eV$ (see Fig. S3-II).

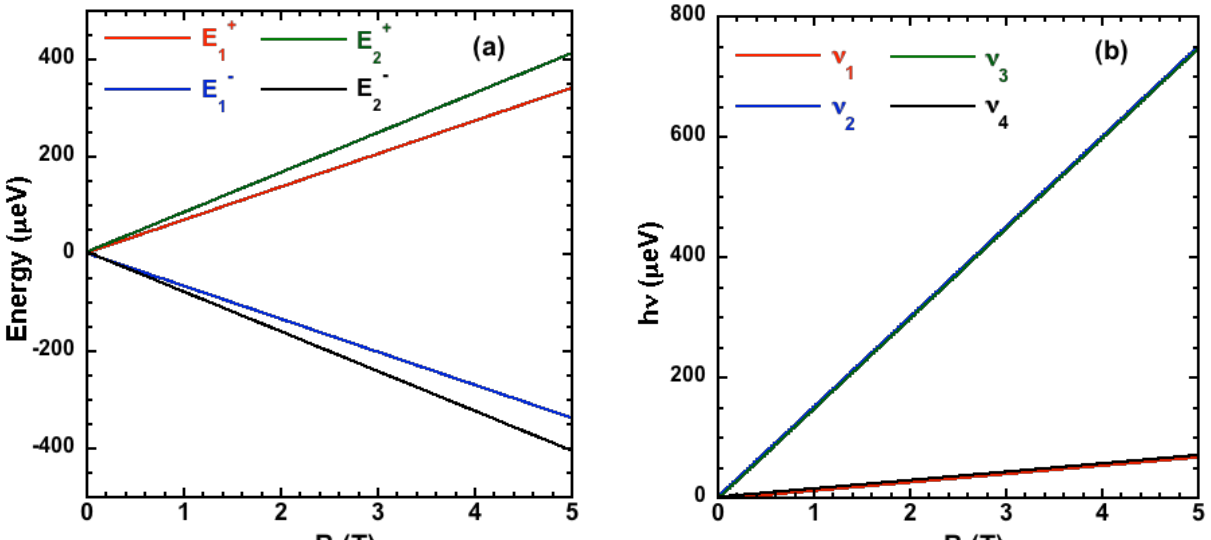

Fig. S3-II : (a) Energies of the four excitonic states versus magnetic field ; (b) oscillation frequencies of the exciton spin component for a tetragonal crystal and a FSS defined by $\delta_{BD} = 5\ \mu eV$ and $\Delta E = -1\ \mu eV$ according to Ref. [4]. The Landé factors are $g_e = 2.59$ and $g_h = 0.24$.

In a tetragonal symmetry, the FSS in MAPbI3 has been estimated and is given by $\delta_{BD} = 300\ \mu eV$, $\Delta E = 126\ \mu eV$ [3]. Fig. S3-III shows the magnetic-field dependence of the four frequencies. A clear non-linear behavior is observed for all the frequencies.

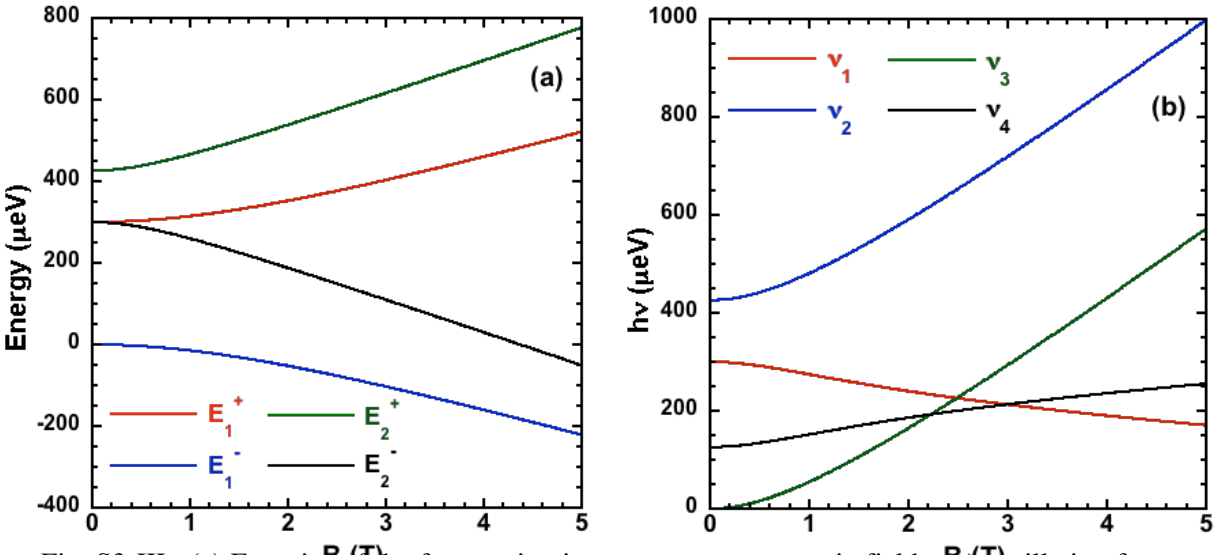

Fig. S3-III : (a) Energies of the four excitonic states versus magnetic field ; (b) oscillation frequencies of the exciton spin component for a tetragonal crystal and a FSS given by $\delta_{BD} = 300\ \mu eV$ and $\Delta E = 126\ \mu eV$ according to Ref. [3] the Landé factors are $g_e = 2.59$ and $g_h = 0.24$.

In the orthorhombic phase, present at low temperature, an extra crystal field induces a coupling between the six lowest conduction bands. This leads to a full lift the FSS degeneracy (as illustrated in Fig.S3-I, D_{2h}) so that $E_X \neq E_Y$ $(\Delta E_1 \neq 0)$. One can extend the previous model, by taking into account this condition. For MAPbI3, the FSS is defined by $\delta_{BD} = 400\,\mu eV$, $\Delta E_1 = 95\,\mu eV$ and $\Delta E_2 = 205\,\mu eV$ [3]. The excitonic energies and oscillation frequencies are shown on Fig. S3-IV. As for the tetragonal phase, no linear dependence is observed for the frequencies.

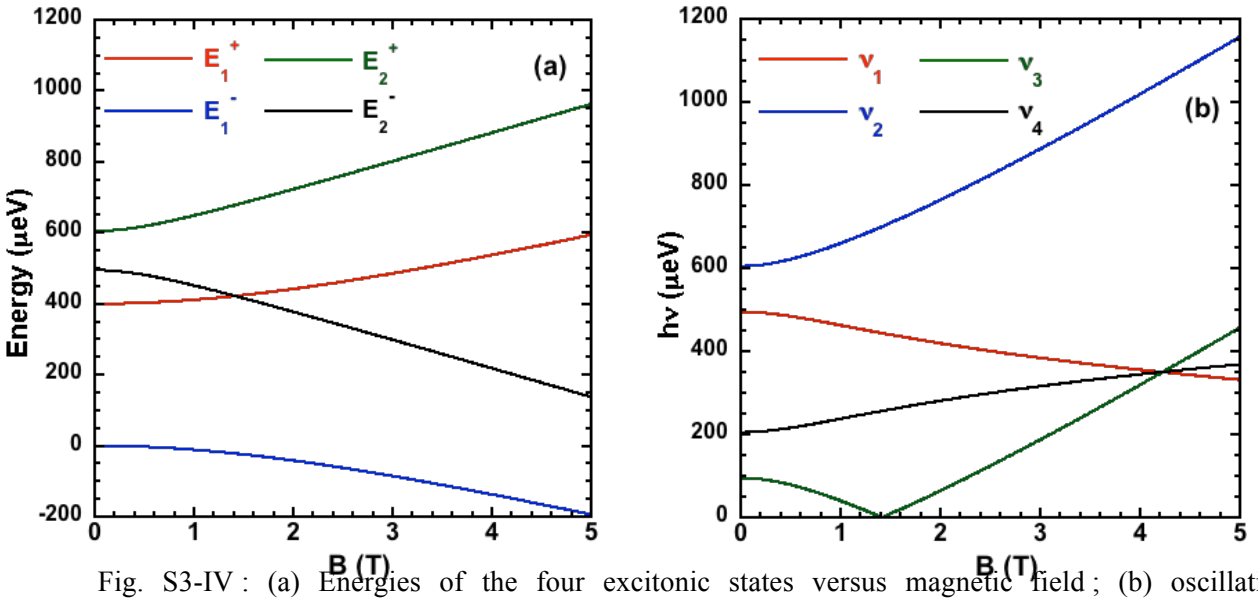

Fig. S3-IV : (a) Energies of the four excitonic states versus magnetic field ; (b) oscillation frequencies of the exciton spin for an orthorhombic crystal and a FSS given by $\delta_{BD} = 400\,\mu eV$, $\Delta E_1 = 95\,\mu eV$ and $\Delta E_2 = 205\,\mu eV$ according to Ref. [3]. The Landé factors are g_e = 2.59 and g_h = 0.24.

4. Evolution of the amplitudes with the magnetic field

The linear dependence of the Larmor precession frequencies with the magnetic field is the principal proof that the observed oscillations do not correspond to exciton quantum beatings in perovskite materials. As it has been demonstrated in $CsPbBr_3$ [5] the observed excited species could correspond instead to carriers bound to impurities (donors or acceptors).

When a circularly polarized light is absorbed by the sample, the optically oriented photo-created electron-hole pairs rapidly are traped, they mainly create donor-bound excitons, denoted D^0X, and acceptors-bound-excitons, denoted A^0X. Donor-bound excitons (acceptors-bound excitons) are complex constituted by three particles, a photo-created electron-hole pair

and a resident electron (hole). After recombination of bound excitons we obtain the resident electron (hole) state.

Since optically oriented excitons can be trapped by donors or acceptors and partially preserved their original spin orientation, we assume the creation of spin-polarized excited-states that transfer subsequently their spin polarization to resident electrons (denoted D^0) and holes (denoted A^0). The essential condition for this spin transfer to fundamental states is that the spin relaxation time of the photo-created holes (in the case of D^0X) or photo-created electrons (in the case of A^0X) should remain in the same order of magnitude or be smaller than the recombination time of the excited states. This condition seems to be fulfilled since photoluminescence shows lifetimes in ns or tens of ns range [6] and the PFR signal shows decay times shorter or comparable to lifetimes (see Figure S4-III (a)). Then after excitation and fast localization, it appears an unbalance between the spin-polarized populations in the excited and fundamental states.

In next lines we develop a two-level system that suppose the creation of an initial spin polarization in both excited (bound exciton) and fundamental states (bound carriers). The next equations model the spin dynamics observed for a single excited species:

$$\frac{d\vec{S}_e}{dt} = \vec{\Omega}_e \times \vec{S}_e - \Gamma_e \vec{S}_e \qquad \text{S4.1 (a)}$$

$$\frac{d\vec{S}_f}{dt} = \vec{\Omega}_f \times \vec{S}_f + \gamma_e \vec{S}_e - \gamma_f \vec{S}_f \qquad \text{S4.1(b)}$$

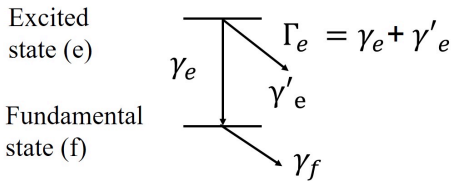

Fig. S4-I Scheme labelling the spin relaxation and recombination rates involved in the spin dynamics of a two level system.

where $\vec{S}_f$, γ_f, $\vec{\Omega}_f$ ($\vec{S}_e$,Γ_e, $\vec{\Omega}_e$) correspond to the spin polarization, relaxation rate and precession frequency of the fundamental state (excited state). The term γ_e manifests a possible transfer of the spin polarization from the excited to the fundamental state, and the term γ'_e includes the spin relaxation and non-radiative processes of the excited states.

The signal associated to a single two-level system (exciton bound to donor and electron bound to donor, or exciton bound to acceptor and hole bound to acceptor) is then given by the next expression:

$$S(t) = R_1 \cos(\Omega_e t - \alpha_1)\, e^{-\Gamma_e t} + R_2 \cos(\Omega_f t - \alpha_2) e^{-\gamma_f t} \quad \text{(S4. 2)}$$

with the amplitudes of each state written:

$$R_1 = \frac{\sqrt{(\Gamma_e-\gamma_f-\gamma_e)^2+(\Omega_f-\Omega_e)^2}}{\sqrt{(\Gamma_e-\gamma_f)^2+(\Omega_f-\Omega_e)^2}} S_{ex}(0), \quad R_2 = \frac{\sqrt{(\Gamma_e-\gamma_f+\gamma_e R_0)^2+(\Omega_f-\Omega_e)^2}}{\sqrt{(\Gamma_e-\gamma_f)^2+(\Omega_f-\Omega_e)^2}} S_{fx}(0) \qquad \text{(S4. 3)}$$

with $S_{ex}(0)$ ($S_{fx}(0)$) the initial polarization of the excited (fundamental) state and R_0 given by: $R_0 = S_{ex}(0)/S_{fx}(0)$.

We assume that at the peak of the absorption spectrum, both species are detected with different amplitudes in PFR. These amplitudes are related to the initial polarization $S_{ex}(0)$ ($S_{fx}(0)$) but also to the number of donors or acceptors and, at the considered detection energy, to the sensitivity of the PFR signal to the presence of this spin polarization of photo-created and resident carriers. In CdTe quantum wells, it was demonstrated that PFR signal excited and detected at the energy of the free exciton is sensitive to the spin polarization of electrons bound to donors [7].

Since an exciton can be trapped by a donor or an acceptor, we suppose the creation of a spin polarization in both excited and fundamental states. When the exciton is trapped by a donor, the fundamental (excited) state oscillates at the electron (hole) frequency $\Omega_f^{D^0} = \omega_e$ ($\Omega_e^{D^0X} = \omega_h$), meanwhile when the exciton is trapped by an acceptor the fundamental (excited) state oscillates at the hole (electron) frequency $\Omega_f^{A^0} = \omega_h$ ($\Omega_e^{A^0X} = \omega_e$).

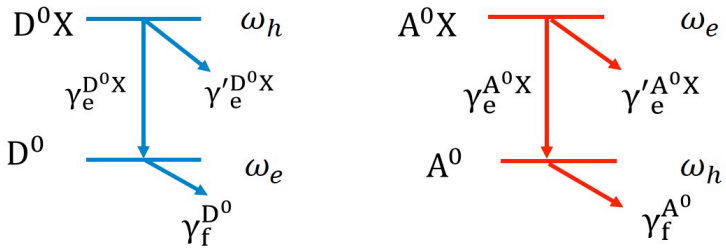

Fig. S4-II Scheme modeling a 4-level system when an exciton is trapped by a donor or an acceptor

From the PFR signal at B = 0 obtained at the peak of the absorption spectrum we observe a fast component that relaxes in a time of 100 ps and a long component that relaxes in 2.8 nanoseconds (see Figure S4 III (a)). Within this framework, we associate the short relaxation time $1/\Gamma_e$ to D^0X or A^0X species, and the long relaxation times to a combination of the relaxation of the two fundamental states: donor-bound electrons $1/\gamma_f^{D^0}$ and acceptor-bound holes $1/\gamma_f^{A^0}$ (of the same order as $T_{2,i}(0)$ obtained by extrapolation to zero magnetic field).

Fig. S4-III (b) shows the amplitudes obtained from the fit of the PFR signal at different values of the magnetic field, fitted with Eq. (1) of the main text. We assume that the excited state for donors and acceptors disappears in a very short time, as evidence by the PFR signal, and then the amplitudes that we observed correspond to the amplitudes of the fundamental states (electron or hole bound to donor or acceptor, respectively). We associate the electron amplitude to the one of a fundamental state in a donor system:

$$R_2^{D^0} \propto \frac{\sqrt{\left(\Gamma_e^{D^0X} - \gamma_f^{D^0} + \gamma_e^{D^0X}\mathrm{R}_0\right)^2 + (\omega_e - \omega_h)^2}}{\sqrt{\left(\Gamma_e^{D^0X} - \gamma_f^{D^0}\right)^2 + (\omega_e - \omega_h)^2}} S_f^{D^0}(0), \qquad \text{(S4.5a)}$$

and the hole amplitude to the fundamental state in an acceptor system:

$$R_2^{A^0} \propto \frac{\sqrt{\left(\Gamma_e^{A^0X} - \gamma_f^{A^0} + \gamma_e^{A^0X}\mathrm{R}_0\right)^2 + (\omega_h - \omega_e)^2}}{\sqrt{\left(\Gamma_e^{A^0X} - \gamma_f^{A^0}\right)^2 + (\omega_h - \omega_e)^2}} S_f^{A^0}(0), \qquad \text{(S4.5b)}$$

The values of the parameters corresponding to the dashed lines in figure S4 III (b) appear in the Table S4. We can remark that the decreasing behavior of the electron contribution and the constant one of the hole, is well described by this model. This behavior is very different from the one proposed in Ref. [4] for exciton beatings.

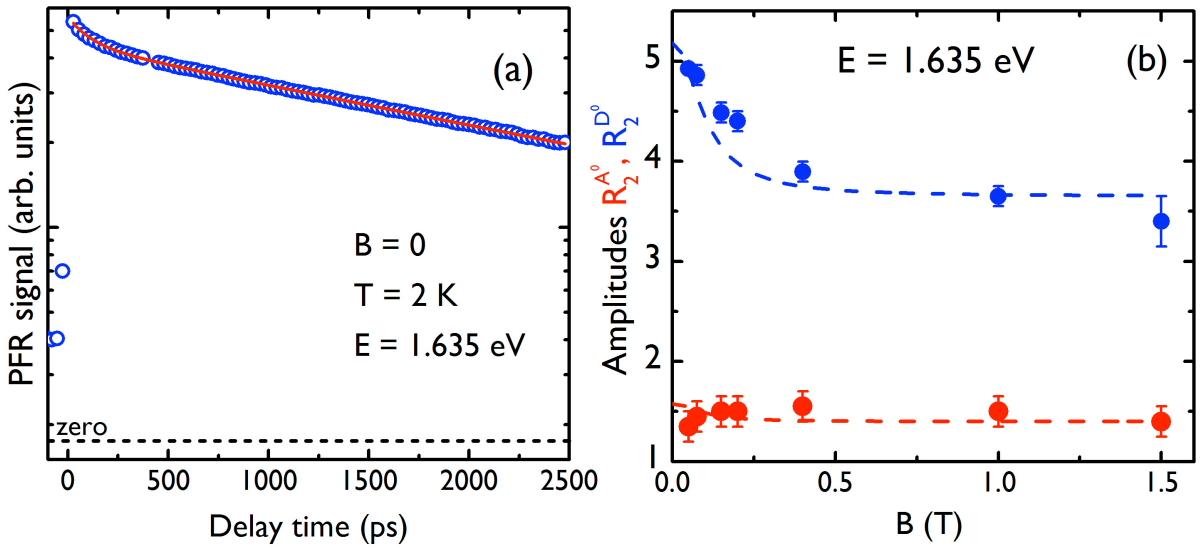

Fig S4-III (a) PFR signal at B = 0 as a function of the time delay between the pump and probe pulses obtained at the peak energy of the absorption spectrum. (b) Amplitudes vs magnetic field obtained from the fit of Eq. (1) (main text) to the PFR signal at different magnetic fields (see Fig. 2 of the main text). The dashed lines represent the evolution in magnetic field

assuming that the observed relaxation time corresponds to donor-bound electrons (blue dashed line) and acceptor-bound holes (red-dashed line).

Exciton trapped by	*Excited states*				*Fundamental states*		
Donor	$\Gamma_e^{D^0X}$ *(1/ps)*	$\gamma_e^{D^0X}$ *(1/ps)*	$S_e^{D^0X}$ *(0)*	ω_h *(rad/ps)*	$\gamma_f^{D^0}$ *(1/ps)*	$S_f^{D^0}(0)$	ω_e *(rad/ps)*
	0.02	0.01	3	0.02 B	2.27×10^{-4}	3.65	0.23 B
Acceptor	$\Gamma_e^{A^0X}$ *(1/ps)*	$\gamma_e^{A^0X}$ *(1/ps)*	$S_e^{A^0X}$	ω_e *(rad/ps)*	$\gamma_f^{A^0}$ *(1/ps)*	$S_f^{A^0}(0)$	ω_h *(rad/ps)*
	0.02	0.01	*0.35*	0.23 B	2.68×10^{-4}	*1.4*	0.02*B

Table S4: Parameters used to model the evolution of the amplitudes with the magnetic field, extracted from the fit of the PFR signal obtained at the peak of the absorption spectrum. The relaxation rates $\gamma_f^{D^0}$, $\gamma_f^{A^0}$ and Larmor precession frequencies have been determined experimentally (see main text).

The evolution of the amplitudes vs magnetic field when the excitation is done at a lower energy, E = 1.612 eV, is shown in Fig. S4-IV. We remark that at this energy the species oscillating at the hole frequency has a more important contribution than the one oscillating at the electron frequency. Within the framework developed above, this behavior could be explained by a higher population of spin-polarized holes bound to acceptors than spin-polarized electrons bound to donors, or by a higher sensitivity of the PFR detection to the spin-polarized hole bound to acceptors, when the excitation is placed at lower energies. However, more studies would be needed in order to reveal the recombination times of the excited species.

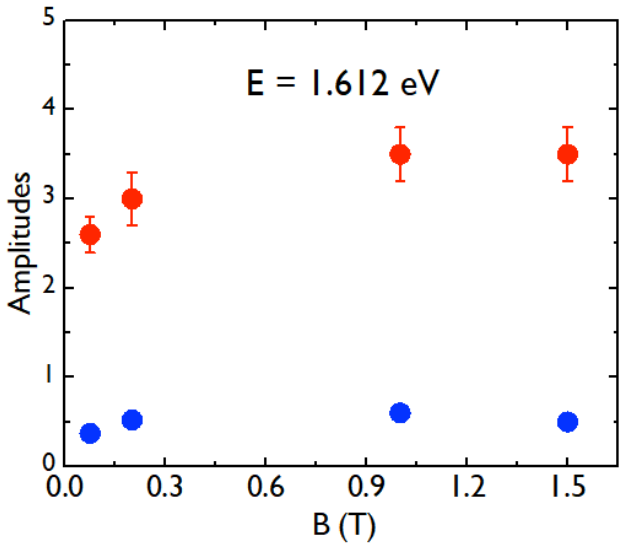

S4-IV Evolution of the amplitudes vs magnetic field obtained from the fit of the PFR signal at different values of a transversal magnetic field with Eq. (4) (see main text) obtained at the energy E =1.612 Ev. Red: hole contribution; blue: electron contribution.

5. EXPERIMENTAL METHODS

MAPI Thin Film Preparation. The samples studied here are polycrystalline films of $CH_3NH_3PbI_3$ prepared from a solution of methyl ammonium iodide (1.5 mmol, 238.5 mg) and lead iodide (1.5 mmol, 691.5 mg) in γ-butyrolactone (2mL). The new quartz substrate was cleaned in a solution of ethanol in an ultrasonic bath during 10 minutes, and then treated by O_2 plasma during 20 minutes. In a glove box, 50 uL of MAPI solution were deposited on the substrate by spin coating at 2000 rpm during 30 s. Then the sample was annealing at 120 °C during 1 minute.

Absorption Spectroscopy. The absorption spectra as a function temperature are presented in Figure S1. Optical transmission spectra were recorded using a CARY 5000 double-beam spectrophotometer (Agilent Company) with 0.4 nm resolution. For temperature-dependent studies, a helium exchange gas cryostat was used. Temperature was monitored between ≈ 11 K and ambient temperature by Si diodes and controlled by heating of the gas.

Micro-photoluminescence. PL experiments were carried using a confocal-like microscope. A frequency doubled picosecond Ti:Sapphire laser operating at 82 MHz is used and tuned at 400 nm for the spectrum shown in Figure S1 (c). The average excitation powers are a few μW in a spot of diameter close to 1.5 μm. The excitation laser beam is focused using a microscope objective with NA = 0.6. The samples are mounted on the cold finger of a cryostat from Oxford Instruments. The luminescence is collected with the same objective and analyzed in an ACTON SP2760i Roper Scientific-Princeton Instruments spectrometer coupled to a nitrogen-cooled SPEC10 (RS-PI) CCD camera (overall spectral resolution of ≈ 50 μeV). The objective, outside the cryostat, is attached to a three-axis piezo stage, allowing to finely scan the sample.

Photo-induced Faraday rotation. To study the spin dynamics of electrons and holes in our samples, we used the time-resolved photo-induced Faraday rotation (PFR) technique. The

light source is a Ti:Sapphire laser beam with a 2-ps pulse duration and a 76 MHz repetition rate, which is split into pump and probe beams. The pump beam is $\sigma+/\sigma-$ modulated at 500 kHz with an electro-optic modulator, in order to avoid nuclear spin polarization by the optical orientation of the electrons. The probe beam is linearly polarized and its intensity is modulated at 3 kHz. The rotation angle of the probe beam polarization is analyzed after transmission of the sample by using an optical bridge. A double lock-in amplifier is used in order to amplify the signal-to-noise ratio. Superconducting split coils immerged in the cryostat are used to apply a magnetic field in Voigt configuration (in the plane of the sample and perpendicular to the light propagation direction).

REFERENCES:

[1] Ben Aich, R.; Saïdi, I.; Ben Radhia, S.; Boujdaria, K.; Barisien, T.; Legrand, L.; Bernardot, F.; Chamarro, M.; C. Testelin, Bright-Exciton Splittings in Inorganic Cesium Lead Halide Perovskite Nanocrystals, *Phys. Rev. Applied* **2019**, 11, 034042.

[2] Ramade, J.; Andriambariarijaona, L. M.; Steinmetz, V.; Goubet, N.; Legrand, L.; Barisien, T.; Bernardot, F.; Testelin, C.; Lhuillier, E.; Bramati, A.; Chamarro, M. Fine structure of excitons and electron–hole exchange energy in polymorphic $CsPbBr_3$ single nanocrystals, *Nanoscale* **2018**,10, 6393-6401.

[3] Ben Aich, R.; Ben Radhia, S.; Boujdaria, K.; Chamarro, M. and Testelin, C. Multiband k.p Model for Tetragonal Crystals: Application to Hybrid Halide Perovskite Nanocrystals, *J. Phys. Chem. Lett.* **2020**, 11, 3, 808–817.

[4] Odenthal, P.; Talmadge, W.; Gundlach, N.; Wang, R.; Zhang, C.; Sun, D.; Yu, Z.- G.; Vardeny, Z. V.; Li, Y. S. Spin-polarized exciton quantum beating in hybrid organic–inorganic perovskites, *Nature Physics* **2017,** 13, 894–899.

[5] Belykh, V. V.; Yakovlev, D. Y.; Glazov, M. M.; Grigoryev, P. S.; Hussain, M.; Rautert, J; Dirin, D. N.; Kovalenko, M. V. and Bayer. M. Coherent spin dynamics of electrons and holes in CsPbBr3 pervoskite crystals, *Nat. Commun*. **2019,** 10, 673

[6] Diab, H.; Trippé-Allard, G.; Ledée, F.; Jemli, K.; Vilar, C.; Bouchez, G.; Jacques, V. L. R.; Tejeda, A.; Even, J.; Lauret, J.-S.; Deleporte, E.; and Garrot, G. Narrow Linewidth Excitonic Emission in Organic–Inorganic Lead Iodide Perovskite Single Crystals. *J. Phys. Chem. Lett.* **2016***,* 7, 24, 5093–5100.

[7] Tribollet, J.; Aubry, E.; Karczewski, G.; Sermage, B.; Bernardot, F.; Testelin, C. and Chamarro, M, Enhancement of the electron spin memory by localization on donors in a CdTe quantum well, *Phys. Rev. B* **2007**, 75, 205304